

## TURBULENT MIXING OF HEAT AND MOMENTUM IN A TURBULENT BOUNDARY LAYER PERTURBED BY AN EFFUSION FILM

**Daniel Burnett**

Department of Aeronautics  
Imperial College London  
London, SW7 2AZ  
d.burnett20@imperial.ac.uk

**Kevin Gouder**

Department of Aeronautics  
Imperial College London  
London, SW7 2AZ  
kevin.gouder04@imperial.ac.uk

**Jonathan F. Morrison**

Department of Aeronautics  
Imperial College London  
London, SW7 2AZ  
j.morrison@imperial.ac.uk

### ABSTRACT

Next generation gas turbine engines using effusion cooling require detailed measurements of the turbulent mixing of temperature and momentum, to improve modelling in RANS simulations and maximise efficiency gains. Most studies focus on empirical correlations for the film effectiveness, which tend to be highly dependent on velocity ratio and geometry. Detailed flowfield and turbulent mixing measurements are scarce and the mechanisms behind these processes are not well understood (Han, 2013). The majority of previous studies focus on film cooling and not effusion cooling, where the mechanisms are observed to be different (Krewinkel, 2013). Therefore, an experiment was conducted in the 10x5 wind tunnel, to enable high spatial and temporal resolution measurements of the momentum and temperature mixing in a large turbulent boundary layer with effusion cooling at low velocity ratios.

It was observed that the effusion film causes a velocity deficit within the boundary layer, coupled with a reduction in skin friction coefficient. These effects were naturally more pronounced for profiles on the centreline of the holes. For a velocity ratio of 0.37, regions of film lift-off were observed, where the temperature and momentum boundary layer structures significantly change to those at lower velocity ratios. Here, the gradient diffusion hypothesis was observed to be violated due to negative heat diffusivity values and consequently, a negative turbulent Prandtl number. The Reynolds analogy was also not valid in the boundary layer overlap region, with turbulent Prandtl number values ranging from 1.1 to 1.4. The film lift-off could be attributed to the formation of contra-rotating vortices either side of the effusion jets. Wall-normal velocity data supports this claim. Peaks in the streamwise velocity variance were found to coincide with peaks in the wall-normal shear production term on the hole centreline. No corresponding peak was measured between holes, which suggests the source of the turbulence here is due to production or transport through spanwise gradients.

### INTRODUCTION

In order to raise the maximum cycle temperature in gas turbine engines for increased thermal efficiency, more effective turbine blade cooling strategies are required. One such method is through the use of effusion cooling - a denser array of smaller diameter holes on the blade surface. This increases internal convective cooling, and has the aerodynamic advantages of less film lift-off, with increased surface film coverage and higher cooling effectiveness. The cooler air is bled from the final compressor stage, which reduces the total available work output and therefore engine efficiency. This creates the challenging problem of sufficiently reducing heat transfer to the blade surface with the minimum amount of coolant usage.

There is a lack of understanding of the mixing processes and mechanisms between the cooler film and hotter freestream, which leads to excessive coolant use in real turbine designs and the concomitant efficiency penalties (Han, 2013). Accurately modelling such flows in RANS simulations, to improve next-generation designs, requires detailed simultaneous measurements of the momentum and scalar fields.

In gas turbine flows, the interaction between large energy-containing structures from combustor-turbine interactions or cooling jets, with fine-scale turbulence, has been shown to lead to poor predictions of turbulent transport in RANS models, and the invalidation of linear momentum and heat diffusivity models (Sandberg and Michelassi, 2022). In regions of a trenced film cooling flow, Shreivogel et al. (2016) found the turbulent heat flux and mean temperature gradient to be in opposite directions, contradicting the gradient diffusion hypothesis. Large departures from a constant value of turbulent Prandtl number of  $Pr_t = 0.85$ , commonly used in RANS simulations, has also been previously observed. Kohli and Bogard (2005) reported  $Pr_t$  values ranging from 0.5 – 2 in a film cooling flow with a single row of holes. Departures from the Reynolds analogy have been documented in other perturbed boundary layer studies (Smits and Wood, 1985). Detailed investigations of the turbulent heat and momentum mixing in multi-row hole geometries, more typical of an effusion cooling flow field, are scarce. In these flows, the interactions of jets in successive rows is strong and causes large deviations in film effectiveness,

from predictions using a linear superposition model (Murray et al., 2018).

The current study involves experiments performed in the 10x5 wind tunnel. It aims to analyse and quantify the turbulent transport of momentum and heat in a moderately high Reynolds number ‘canonical’ incoming turbulent boundary layer ( $\delta_{99} \approx 0.3$  m,  $Re_\tau \approx 6500$ ), perturbed by an effusion film at low velocity ratios ( $VR = U_e/U_\infty < 0.4$ ), and a slightly lower temperature ( $\Delta\Theta \approx 6$  °C), so that temperature can be treated as a passive scalar. Here,  $U_e$  is the exit velocity from the effusion holes. The bulk Richardson number is small, ( $Ri_\delta \approx 0.001$ ), indicating negligible buoyancy effects. A schematic is illustrated in figure 1.

Turbulence intensities reaching 30% in the boundary layer near-wall region (Castro et al., 2013), are similar to those measured at the combustor-turbine interface in real gas turbines (10% – 35%) (Cha et al., 2012). The hole diameters and freestream velocity are increased and reduced respectively by a factor of 16, with respect to typical gas turbine conditions, enabling high resolution simultaneous temperature and velocity measurements, spatially and temporally. The largest length scales observed in a gas turbine after combustion ( $l/D \approx 25$ ), are of similar magnitude to the LSMs observed in turbulent boundary layers ( $\delta_{99}/D \approx 14$ ). The simplified geometry and canonical incoming flow will isolate the effects of the interactions between the film and the incoming flow, to improve modelling of quantities such as the turbulent diffusivities and turbulent Prandtl number in RANS simulations, and consequently improve heat transfer predictions.

## EXPERIMENTAL DETAILS

Simultaneous boundary layer profiles of the temperature, and streamwise and wall-normal velocity components were acquired using a 1  $\mu$ m diameter cold-wire, of length  $l/d = 400$ , and an adjacent x-wire respectively, for 180 s per point and an acquisition frequency of 20 kHz. The wall-normal profiles were acquired at two spanwise locations: along the centreline of a column of holes, where the effects of blowing will naturally be more significant, and between two columns of holes, as indicated in figure 2. The velocity ratios tested were  $VR = 0, 0.10, 0.17, 0.37$ . Cool air was supplied to the plenum using compressed air, fed through a Ranque-Hilsch vortex tube. Details of the working principle of a Ranque-Hilsch vortex tube can be found in the review by Kaufmann (2022). Eight Pt100 temperature sensors were mounted within the holes indicated in figure 2 (white ellipses), to determine the effusion exit temperature, used to normalise the temperature profiles and to examine the temperature uniformity in the plenum.

The x-wire was mounted on a motorised pitching arm and calibrated using the look-up table method. For voltage points outside of the calibration domain, velocities were determined using the effective angle method. See Burattini and Antonia (2005) for more details of the calibration procedure. X-wire voltage measurements ( $E$ ) were corrected for temperature using the instantaneous cold-wire temperature data ( $T$ ), with the formula  $E_{corr} = E \sqrt{(T_w - T_{cal}) / (T_w - T)}$ , where  $T_{cal}$  is the ambient temperature at calibration and  $T_w$  is the hot-wire temperature. The accuracy of the temperature correction and the effects of buoyancy were examined through profiles acquired using Laser Doppler Anemometry (LDA) in an isothermal flow field at  $VR = 0.10, 0.37$  (not shown in plots for clarity). Deviations in the mean streamwise velocity between profiles were found to be within 2%. Upstream boundary layer

profiles were measured using LDA, to provide measurements closer to the wall, than what is possible with the x-wire.

The wall shear stress was measured at a variety of velocity ratios, using oil film interferometry (OFI). Measurements were taken  $0.45\delta$  downstream of the centreline of the last row of holes, as indicated in figure 3, as well as on the immediate upstream boundary layer. The oil kinematic viscosity, responsible for highest uncertainty in the wall shear stress in OFI measurements (Discetti and Ianiro, 2017), was measured with an Ubbelohde capillary viscometer in a constant temperature recirculating water bath, at a range of temperatures with 1 °C increments. The formula  $\nu = Ae^{\alpha\nu T}$  was fitted to the data. Isothermal blowing was used, to reduce the uncertainty in the temperature of the oil film, and therefore its viscosity. The oil temperature used to determine the kinematic viscosity was assumed to be the average of the effusion temperature and freestream temperature, with the difference between them less than  $\pm 0.05$  °C.

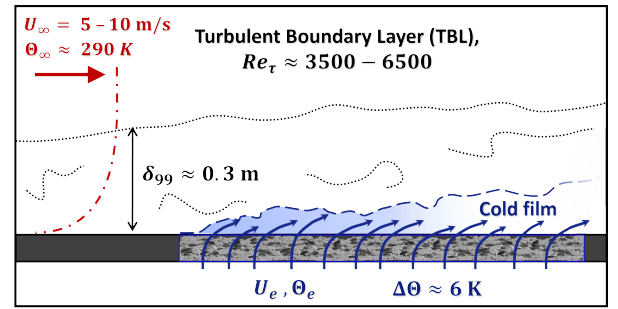


Figure 1: Side view diagram of the experimental setup.

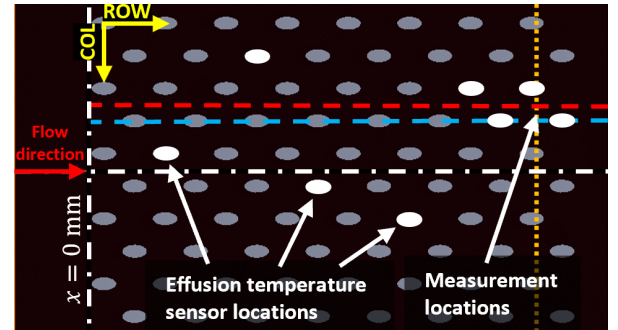


Figure 2: Plan view diagram of the plenum.

## RESULTS AND DISCUSSION

Skin friction coefficient results at range of velocity ratios, normalised by the upstream skin friction coefficient are presented on figure 3. For an individual run, the skin friction coefficient was determined by calculating the rate of change of fringe wavelength across multiple lines of pixels at the centre of the oil drop, and averaged. The error bars in figure 3 represent the 95% confidence interval based on these values. The presence of the effusion panel and the roughness associated with the holes ( $VR = 0$ ) causes a reduction in skin friction coefficient. The addition of blowing is observed to further monotonically reduce the friction coefficient on the centreline of the effusion holes, but remains approximately constant between holes, for  $VR < 0.25$ . At  $VR = 0.37$ , the friction coefficient has begun to plateau on the hole centreline, but increases beyond the upstream value between holes.

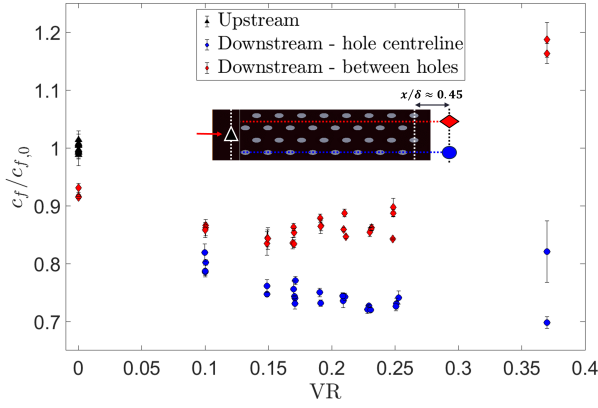


Figure 3: Skin friction coefficient measurements at a variety of velocity ratios, normalised by the upstream skin friction coefficient. Error bars represent the 95 % confidence interval across an individual run.

Figures 4 and 5 show the acquired mean velocity profiles. The addition of the film (at these low velocity ratios) is to cause a velocity deficit within the boundary layer relative to the upstream case, which is consistent with the reduction in skin friction coefficient shown in figure 3. This is due to the low momentum effused fluid penetrating into a region of higher momentum within the boundary layer. For a constant velocity ratio, the velocity deficit along the centreline of the holes (figure 4) is observed to be greater than for the case of between two adjacent columns of holes (figure 5), which is also in agreement with the respective lower skin friction coefficient.

As  $VR$  is increased, the velocity deficit increases and spans across a larger wall-normal distance for  $y/D \gtrsim 1$ , due to higher effusion momentum and increased boundary layer penetration. On the hole centreline, the velocity deficit is still apparent in the near wall region, but the profiles begin to collapse between holes. This is consistent with the skin friction trends previously discussed. For  $VR = 0.37$ , the bulk of the effused fluid starts to lift from the surface on the hole centreline, causing plateaus in the velocity profiles, as seen in figure 4. Between columns of holes, the trend reverses and the velocity increases, potentially due to stronger jets causing viscous blockage and an acceleration of the flow between holes. This could explain the increase in skin friction coefficient at  $VR = 0.37$ . The streamwise velocity differences between the two spanwise locations, for a given wall-normal location, consequently becomes larger with increasing velocity ratio, which suggests an increasing impact of velocity gradients in the spanwise direction ( $\partial U/\partial z$ ) on the flow.

Figures 6 and 7 show the profiles of the variance of the streamwise velocity. In the  $VR = 0$  case, a peak associated with the roughness of the holes is observed at  $y/D \approx 0.25$ . The effect of effusion can be seen to significantly increase momentum mixing away from the wall. On the hole centreline (figure 6), a peak at  $y/D \approx 0.5$  emerges, which moves further from the wall with increasing  $VR$ . This could be associated with the inner  $\overline{u^2}$  peak commonly observed in boundary layers, which was shown not to be present with near wall LDA measurements. For  $VR = 0.37$ , a complex distribution emerges with three peaks in  $\overline{u^2}$  with distinct separation between them. In this case, an inner peak forms at  $y/D \approx 0.1$ , and was not observed in the  $VR = 0.1$  case with either x-wire or LDA measurements. An outer peak also starts to emerge at  $y/D \approx 2$ . The two peaks

become increasingly distinct with increasing  $VR$ , and the outer peak also moves further from the wall with increasing  $VR$ . A single peak in a similar location is seen in the profiles between holes (figure 7). This peak could therefore be associated with the mixing layer at the interface of the film and incoming flow.

The turbulent production and transport of  $\overline{u^2}$  are respectively defined as:

$$P_{uu} = -2 \left[ \overline{u^2} \partial U/\partial x + \overline{uw} \partial U/\partial y + \overline{wv} \partial U/\partial z \right], \quad (1)$$

$$T_{uu} = \partial/\partial x(\overline{u^3}) + \partial/\partial y(\overline{u^2v}) + \partial/\partial z(\overline{u^2w}). \quad (2)$$

Profiles of the wall-normal gradient terms in equations 1 and 2, are presented in figures 8 and 9 respectively, to further understand the  $\overline{u^2}$  distributions shown in figures 6 and 7. In a canonical turbulent boundary layer, this is the only non-zero production of turbulent kinetic energy term. The dominant  $\overline{u^2}$  peak on the hole centreline at  $y/D \approx 0.5$  is seen to be caused by a large peak in the wall-normal shear production term. For  $VR = 0.37$ , there are also peaks in production corresponding to the locations of the two other  $\overline{u^2}$  peaks at  $y/D \approx 0.1$  and  $y/D \approx 2$ . The peaks occur in the regions before/after the mean velocity plateaus, where the shear rate is unsurprisingly higher in these regions.

However no corresponding peak in the wall-normal gradient production or transport terms is observed for the between holes cases. This suggests strong spanwise gradients are responsible for the peak in  $\overline{u^2}$ , either due to production ( $\overline{uw} \partial U/\partial z$ ) or transport ( $\partial/\partial z(\overline{u^2w})$ ) originating from strong fluctuations on the hole centreline. With the film developing over a length of approximately  $3\delta$ , the streamwise gradients are less significant.

Figures 10 and 11 show the corresponding mean and variance temperature profiles respectively. Many of the trends observed in the streamwise velocity profiles are similarly observed here. The mean temperature is lower across the whole thermal boundary layer, as  $VR$  is increased, and in the location along the centreline of the holes. At  $VR = 0.37$ , there are regions where the temperature gradients are negative, due to the bulk of the lower temperature film lifting from the surface. This was also observed in the isothermal scalar light intensity measurements by Basley et al. (2022). The temperature profiles at different spanwise locations collapse at  $y/D \approx 2$ , beyond which the film becomes homogeneous. This is at a similar location to that where the turbulent fluctuations are strongest.

For  $VR \leq 0.17$ , the peaks in  $\overline{\theta^2}$  is observed to increase in magnitude and distance from the wall, due to the increased momentum mixing and higher penetration of the film into the boundary layer. On the hole centreline, the peak in  $\overline{\theta^2}$  occurs in a similar location to the  $\overline{u^2}$  peak at  $y/D \approx 0.5$ , suggesting that the temperature fluctuations could be primarily driven by streamwise velocity fluctuations. This is not observed in the location between holes, where a broad  $\overline{\theta^2}$  peak appears before the  $\overline{u^2}$  peak, centred approximately at  $y/D \approx 0.8$ . The  $v^2$  peak (not shown) occurs in a similar location to the  $\overline{u^2}$  peak, so the temperature fluctuations here could be strongly influenced by spanwise velocity fluctuations.

For  $VR = 0.37$ , where flow dynamics are seen to change considerably, the  $\overline{\theta^2}$  profiles also change in distribution. The magnitude of the peak for the hole centreline case does not increase, although this could be due to the upstream boundary

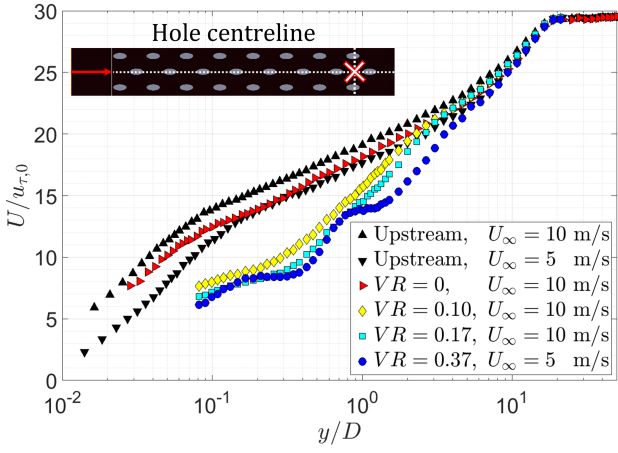


Figure 4: Mean streamwise velocity profiles on the centreline of a column of holes.

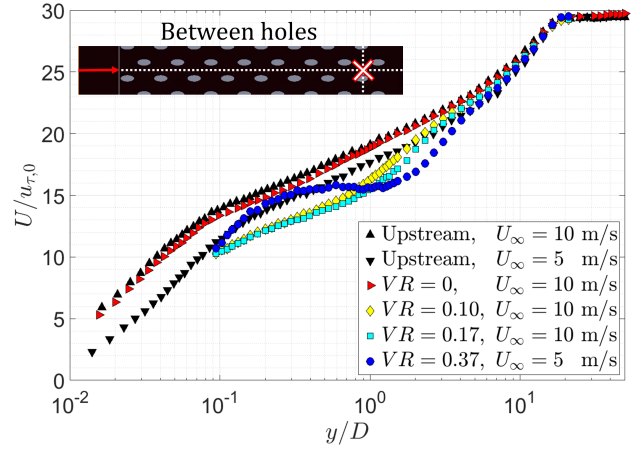


Figure 5: Mean streamwise velocity profiles between adjacent columns of holes.

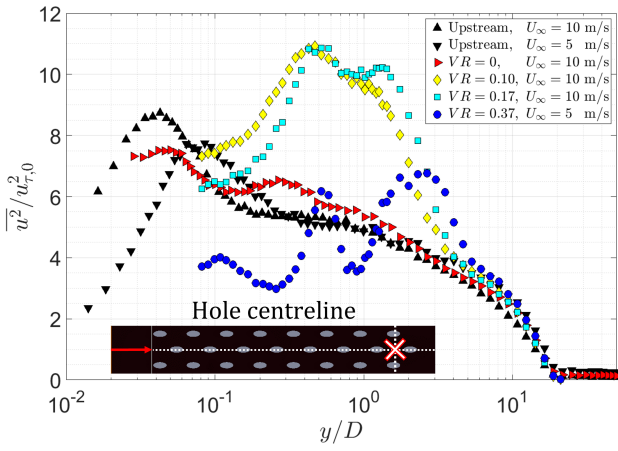


Figure 6: Mean streamwise velocity profiles on the centreline of a column of holes.

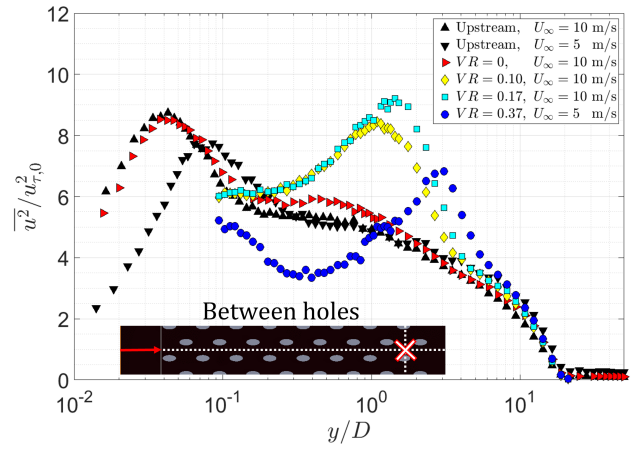


Figure 7: Mean streamwise velocity profiles between adjacent columns of holes.

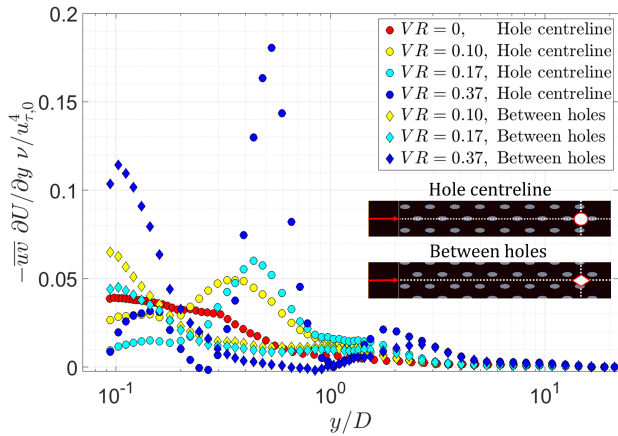


Figure 8: Wall-normal profiles of the turbulent production term  $\overline{wv} \partial U / \partial y$ .

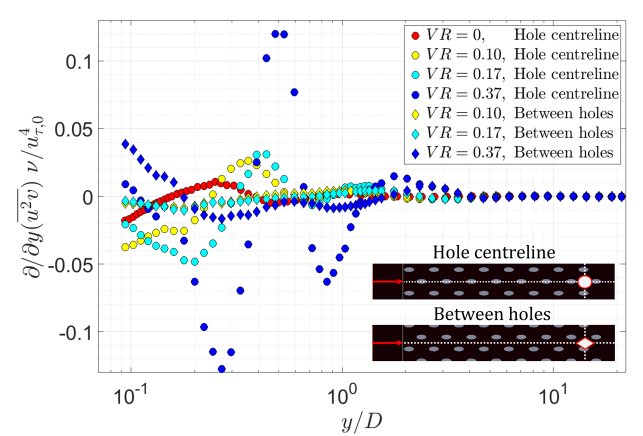


Figure 9: Wall-normal profiles of the turbulent diffusion term  $\partial / \partial y (\overline{u^2 v})$ .

layer being at a lower Reynolds number, with reduced turbulent fluctuations (not accounted for in this scaling). However, the region of high temperature fluctuations is observed to extend over a much greater wall-normal region, as well as the emergence of a second peak in  $\overline{\theta^2}$ . There is conversely a large increase in magnitude of the  $\overline{\theta^2}$  peak between holes.

A possible mechanism for the film lift-off at  $VR = 0.37$

can be explained through figure 12. Measurements aligned with the centreline of the holes show a positive wall-normal velocity, which increases with increasing  $VR$ . For measurements in between two columns of holes,  $V$  is observed to be closer to zero, and becomes negative for  $VR = 0.37$ . This could be attributed to contra-rotating vortices, formed either side of the the individual effusion jets, which would cause a downwash

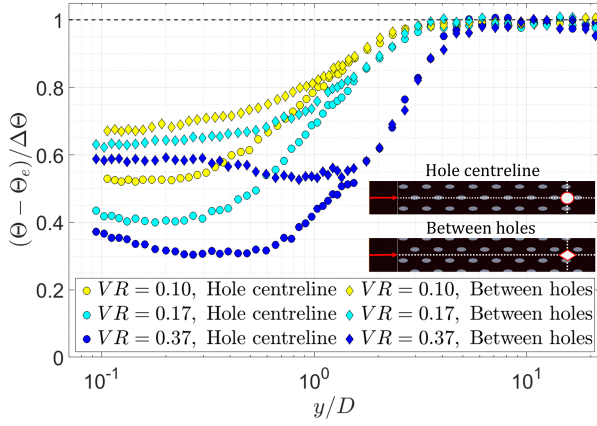


Figure 10: Mean temperature profiles, normalised with respect to the freestream temperature and effusion temperature.

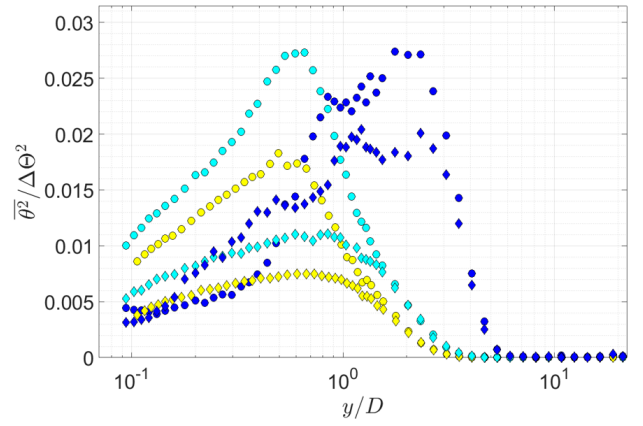


Figure 11: Temperature variance profiles, normalised by the freestream and effusion temperature difference.

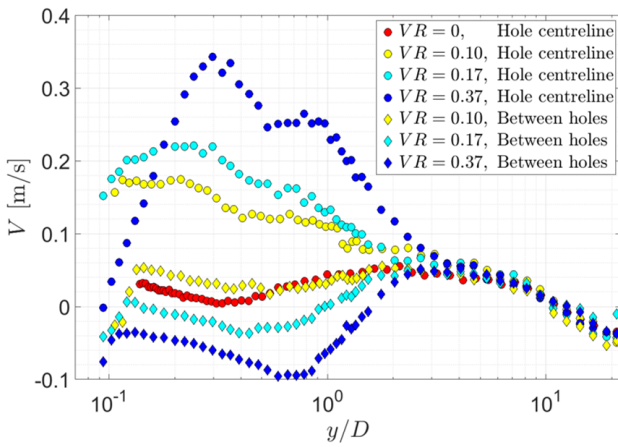


Figure 12: Mean profiles of the wall-normal velocity.

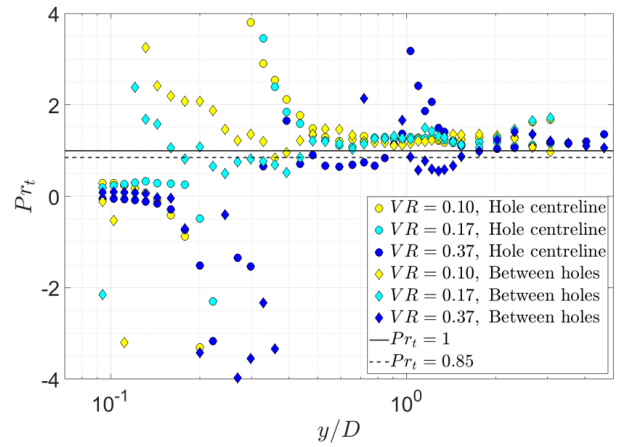


Figure 13: Turbulent Prandtl number profiles.

in the region between two columns. This jet-in-crossflow type phenomenon has been well documented in literature for film cooling flows at high velocity ratios ( $VR > 1$ ), and conjectured to be the dominant mechanism in film lift-off (Zhang et al., 2020). The mechanism is not usually associated with low velocity ratio effusion cooling flows, but seems to be correlated with the observed film lift-off observed in the  $VR = 0.37$  case. Induced vortical structures could also explain the comparatively large increase in temperature fluctuations in the location between holes.

Turbulent Prandtl number profiles are presented in figure 13, where  $Pr_t = \varepsilon_m / \varepsilon_t = (\overline{uv} \partial \Theta / \partial y) / (\overline{v\theta} \partial U / \partial y)$ . They show large departures from the Reynolds analogy ( $Pr_t = 1$ ), and the commonly used  $Pr_t = 0.85$  in commercial CFD codes, which has been obtained from measurements in the logarithmic region of canonical temperature boundary layers (Kays, 1994). A region resembling a logarithmic profile is observed in the mean temperature profiles of figure 10, and the collapse of  $Pr_t$  is good here, but  $Pr_t$  is found to lie primarily between 1.1 and 1.4. Despite some scatter in the data, arising due to uncertainty amplification where the temperature and velocity gradients are close to zero,  $Pr_t$  shows distinct trends with significant variations, ranging from -4 to 4 in the near wall region. Where the temperature profiles plateau in the hole centreline cases, and lift off in both  $VR = 0.37$  cases,  $Pr_t$  is negative. This is due to a negative heat diffusivity, where the turbulent heat flux  $-\overline{v\theta}$  and temperature gradients are in opposite directions.

This directly contradicts the gradient diffusion hypothesis.

## CONCLUSIONS

Simultaneous instantaneous temperature, streamwise and wall-normal velocity measurements were carried out in a large turbulent boundary with effusion cooling at velocity ratios  $VR = 0, 0.10, 0.17, 0.37$ . The low momentum effusion film penetrates into a region of higher velocity in the boundary layer, causing a velocity deficit within the boundary layer, relative to the upstream boundary layer. This velocity deficit was expectedly found to be greater in the location on the hole centreline and with increasing velocity ratio. Skin friction measurements using oil film interferometry showed an associated reduction in skin friction coefficient and supported trends observed in the mean velocity profiles. The mean streamwise velocity and temperature profiles show the film primarily attached to the surface at  $VR = 0.17$ , but lifting from the surface at  $VR = 0.37$ , indicating that there exists a critical velocity ratio in the range  $0.17 < VR < 0.37$ . At  $VR = 0.37$ , this consequently causes an increase in mean streamwise velocity between holes, along with an increase in skin friction coefficient, likely due to an acceleration of the flow between jets.

The lift-off is potentially attributed to contra-rotating vortices formed through a jet-in-crossflow type mechanism. In the location aligned with the centreline of the holes, positive wall-normal velocities were observed, becoming negative for

$VR = 0.37$  in the location between two columns of holes, as would be expected from the formation of such vortices. In the regions where film lift-off was observed, or where the temperature gradients in the near wall region were very small on the hole centreline, turbulent Prandtl number profiles showed that the gradient diffusion hypothesis was invalid. This was due to the temperature gradients and the turbulent heat flux being in opposite directions. Even in the boundary layer overlap/ outer region, the Reynolds analogy is not valid, with  $Pr_t$  ranging from 1.1 to 1.4.

Effusion was found to significantly enhance turbulent fluctuations away from the wall, with the peaks moving further from the wall with increasing velocity ratio. Peaks in the streamwise velocity variance were found to coincide with peaks in wall-normal shear production on the hole centreline. The turbulence generation mechanism is different between holes, where no peaks were observed in the wall-normal production or transport terms. It is likely that spanwise gradients cause the increase in turbulence here, but 3-component data are required to confirm this.

## REFERENCES

- Basley, Jérémy, Gouder, Kevin & Morrison, Jonathan F. 2022 Mixing and large-scale modulation of a turbulent boundary layer perturbed by an effusion film. In *12th International Symposium on Turbulence and Shear Flow Phenomena (TSFP12)*.
- Burattini, P. & Antonia, R. A. 2005 The effect of different x-wire calibration schemes on some turbulence statistics. *Experiments in Fluids* **38** (1), 80–89.
- Castro, Ian P., Segalini, Antonio & Alfredsson, P. Henrik 2013 Outer-layer turbulence intensities in smooth- and rough-wall boundary layers. *Journal of Fluid Mechanics* **727**, 119–131.
- Cha, Chong M., Ireland, Peter T., Denman, Paul A. & Savarianandam, Vivek 2012 Turbulence levels are high at the combustor-turbine interface. American Society of Mechanical Engineers.
- Discetti, Stefano & Ianiro, Andrea 2017 *Experimental aerodynamics*. Boca Raton: CRC Press, includes bibliographical references and index.
- Han, Je-Chin 2013 Fundamental gas turbine heat transfer. *Journal of Thermal Science and Engineering Applications* **5** (2), 021007.
- Kaufmann, André 2022 *The Ranque Hilsch Vortex Tube Demystified Understanding the Working Principles of the Vortex Tube*, 1st edn. Cham: Springer International Publishing.
- Kays, William M. 1994 Turbulent Prandtl number—where are we? *Journal of Heat Transfer* **116** (2), 284–295.
- Kohli, Atul & Bogard, David G. 2005 Turbulent transport in film cooling flows. *Journal of Heat Transfer* **127** (5), 513–520.
- Krewinkel, R. 2013 A review of gas turbine effusion cooling studies. *International Journal of Heat and Mass Transfer* **66**, 706–722.
- Murray, Alexander, Ireland, Peter, Wong, Tsun, Tang, Shaun & Rawlinson, Anton 2018 High resolution experimental and computational methods for modelling multiple row effusion cooling performance. *International Journal of Turbomachinery, Propulsion and Power* **3** (1), 4.
- Sandberg, Richard D. & Michelassi, Vittorio 2022 Fluid dynamics of axial turbomachinery: Blade- and stage-level simulations and models. *Annual review of fluid mechanics* **54** (1), 255–285, uSDOE.
- Schreibvogel, P., Abram, C., Fond, B., Straußwald, M., Beyrau, F. & Pfitzner, M. 2016 Simultaneous khz-rate temperature and velocity field measurements in the flow emanating from angled and trenched film cooling holes .
- Smits, A. J. & Wood, D. H. 1985 The response of turbulent boundary layers to sudden perturbations. *Annual review of fluid mechanics* **17** (1), 321–358.
- Zhang, Jing-Zhou, Zhang, Shengchang, Wang, Chun-hua & Tan, Xiao-Ming 2020 Recent advances in film cooling enhancement: A review. *Chinese Journal of Aeronautics* **33**, 1119–1136.